

Article

Optimization of Parameters for Rheological Properties and Strength of Cemented Paste Backfill Blended with Coarse Aggregates

Jiandong Wang¹, Aixiang Wu¹, Zhuen Ruan^{1,2,*} , Raimund Bürger³, Yiming Wang^{1,4}, Shaoyong Wang^{1,4}, Pingfa Zhang⁵ and Zhaoquan Gao⁵

- ¹ School of Civil and Resource Engineering, University of Science and Technology Beijing, Beijing 100083, China; 15201451814@163.com (J.W.); wuaixiang@126.com (A.W.); ustbwym@126.com (Y.W.); wangshaoyong@ustb.edu.cn (S.W.)
- ² Shunde Graduate School of University of Science and Technology Beijing, Foshan 528399, China
- ³ CI²MA and Departamento de Ingeniería Matemática, Facultad de Ciencias Físicas y Matemáticas, Universidad de Concepción, Casilla 160-C, Concepción 4070371, Chile; rburger@ing-mat.udec.cl
- ⁴ Key Laboratory of High-Efficient Mining and Safety of Metal Mines of the Ministry of Education, University of Science and Technology Beijing, Beijing 100083, China
- ⁵ Chifeng NFC Baiyinnuoer Mining Co., Ltd., Baarin Left Banner, Chifeng 025450, China; zskyzpf@163.com (P.Z.); zskygzq@163.com (Z.G.)
- * Correspondence: ustb_ruanzhuen@hotmail.com

Abstract: Cemented paste backfill (CPB) technology is widely used for environmental protection and underground goaf treatment. The influences of solid concentration, coarse aggregates dosage, and cement dosage on the rheological properties and compressive strength of CPB blended with coarse aggregates (CA-CPB) are investigated through three-factor and four-level orthogonal experiments. The dynamic shear stress and plastic viscosity are selected to characterize the rheological properties of CA-CPB. The uniaxial compressive strength (UCS) is used to describe the compressive strength. The effect of each factor on rheological properties is different from that on UCS. The most significant influences on rheological properties and UCS are solid concentration and cement dosage, respectively. The optimal levels of each factor for rheological properties and UCS are different, resulting in different optimal combinations obtained through range analysis. Therefore, the overall desirability function approach is employed to perform multiple response optimization. The optimal parameters for high fluidity and strength obtained provide valuable information for the CA-CPB process in the Chifeng Baiyinnuoer Lead and Zinc Mine.

Keywords: rheological properties; uniaxial compressive strength; cemented paste backfill; coarse aggregates; waste rock; multiple response optimization



Citation: Wang, J.; Wu, A.; Ruan, Z.; Bürger, R.; Wang, Y.; Wang, S.; Zhang, P.; Gao, Z. Optimization of Parameters for Rheological Properties and Strength of Cemented Paste Backfill Blended with Coarse Aggregates. *Minerals* **2022**, *12*, 374. <https://doi.org/10.3390/min12030374>

Academic Editor: Abbas Taheri

Received: 16 February 2022

Accepted: 15 March 2022

Published: 18 March 2022

Publisher's Note: MDPI stays neutral with regard to jurisdictional claims in published maps and institutional affiliations.



Copyright: © 2022 by the authors. Licensee MDPI, Basel, Switzerland. This article is an open access article distributed under the terms and conditions of the Creative Commons Attribution (CC BY) license (<https://creativecommons.org/licenses/by/4.0/>).

1. Introduction

Tailings generated during the ore processing and waste rock are the main solid wastes in the mining industry [1,2]. Cemented paste backfill (CPB) technology is widely used for environmental protection and underground goaf treatment [3]. In the CPB process, low-concentration tailings' slurry is thickened and dewatered to a high-concentration slurry, and then mixed with cement to prepare a paste with non-stratification, non-segregation, and non-bleeding. After transportation to goaf through pipelines, paste slurry will be solidified to a filling-body to support goaf proof. With CPB technology, solid waste (tailings) is used to deal with the two major hazard sources (tailings dam and goaf), which is called "one waste to cure two harms" [3–5].

High fluidity and high strength are the main requirements for CPB [6]. As the spread and slump are related to the rheological properties [7–9], many scholars adopted rheological properties to characterize the fluidity. Therefore, much research has been conducted

to investigate the rheological properties and compressive strength of CPB through experiments, theoretical analysis, and simulation. The rheological properties of CPB are very complicated and significantly influenced by many parameters. These include the solid concentration [10–12], cement/tailings ratio [11,13], particle size distribution (PSD) of tailings [14], time [13,15,16], temperature [11,15–17], superplasticizer type and dosage [13,18], flocculants dosage [19], cement hydration [13,17], water content and water type [20], shear history [21], and interparticle interactions due to flocculation [22]. At the same time, it is well known that the effects of the solid components [10,23], binder type and dosage [24–27], tailings PSD [28], superplasticizer type and dosage [6], sulfide [29,30], curing conditions (stress, time, and temperature) [16,19,31,32], layered effect [33], and flocculant dosage [34] on the strength of CPB are substantial.

Moreover, some studies show that coarse aggregates (CAs) play an essential role in determining the rheological properties of fluid-solid mixtures such as concrete and debris flows [35,36]. The CAs affect the yield stress through the effective volumetric solid concentration, which can be refined by the size, shape, PSD, and concentration of CAs [35]. It was also found that the rheological properties of the concrete and lubrication layer highly depend on the size of CAs when concrete is being pumped [37]. At the same time, the strength of concrete is greatly influenced by the CAs, including the content, size, surface morphology, structure, and mineralogical component of the CAs [38–40].

Inspired by the above works, waste rocks were used as coarse aggregates to adjust the rheological properties and compressive strength of CPB. We investigated the influence of solid (tailings, CAs, and cement) concentration (SC), CAs dosage (CAsD), and cement dosage (CD) on the rheological properties and compressive strength of CPB blended with coarse aggregates (CA-CPB). Moreover, we optimized parameters for the rheological properties and compressive strength of CA-CPB.

The rest of this paper is structured as follows. In Section 2, the materials and methods, including the properties of the solid materials (tailings, CAs, and cement), methods of the rheological properties test and uniaxial compressive strength (UCS) test, orthogonal experiment design, and test procedure, are introduced. The overall performance, range analysis, and multiple response optimization are shown and discussed in Section 3. In Section 4, we draw conclusions based on the results and discussions.

2. Materials and Methods

2.1. Materials

The tailings were sampled from the Chifeng Baiyinnuoer Lead and Zinc Mine located in the northeast of China. The waste rocks sampled from the same deposit were used as CAs. The commercial ordinary portland cement 42.5 (P.O. 42.5) provided by Zhongshan Group, Zibo, China, was used as the binder. The density, bulk density, and tapped density of tailings, CAs, and cement are shown in Table 1. The PSDs of the tailings and cement analyzed by laser diffraction (TopSizer, OMEC, Zhuhai, China) are shown in Figure 1. The amounts of the tailings and cement <200 μm are 85.94% and 95.48%, respectively. The PSD of the CAs tested through the sieving method is given in Table 2. The PSD of the CAs were mainly in the range of 2500 μm to 10,000 μm . The amount of 8000–10,000 μm CAs content is about 55.69%.

Table 1. Density, bulk density, and tapped density of solid materials.

Materials	Density (g cm^{-3})	Bulk Density (g cm^{-3})	Tapped Density (g cm^{-3})
Tailings	2.74	1.449	1.951
Coarse aggregates	2.52	1.429	1.647
Cement	3.09	1.022	1.384

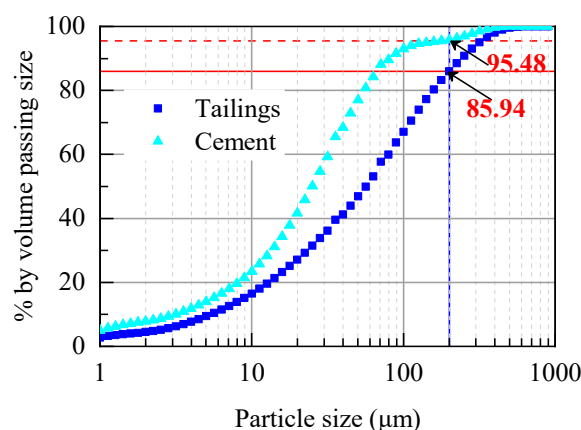


Figure 1. PSDs of tailings and cement.

Table 2. PSD of the coarse aggregates.

Particle Size (μm)	Mass Content (%)
+8000–10,000	55.69
+7000–8000	14.83
+6000–7000	6.80
+5000–6000	8.87
+2500–5000	12.71
+1250–2500	0.32
+315–1250	0.06
–315	0.71

The chemical composition analysis of the tailings, CAs, and cement was performed by X-Ray Fluorescence (XRF). The results are given in Table 3. The main components of the solid materials were SiO_2 , CaO , MgO , Al_2O_3 , and Fe_2O_3 .

Table 3. Chemical components of solid materials.

Chemical Component	SiO_2 (%)	CaO (%)	MgO (%)	Al_2O_3 (%)	Fe_2O_3 (%)	SO_3 (%)	K_2O (%)	TiO_2 (%)	MnO (%)	Others (%)
Tailings	39.18	35.89	3.49	6.99	10.23	0.19	1.28	0.32	2.42	0.01
Coarse aggregates	23.51	59.00	2.41	5.56	7.11	0.35	1.20	0.33	0.51	0.02
Cement	29.12	50.86	2.14	9.06	3.29	3.47	1.27	0.62	0.16	0.01

2.2. Test/Methods

An ICAR rheometer (Germann Instruments) was used to test the rheological parameters of CA-CPB. The ICAR rheometer consists of a container, a motor drive with a torque meter unit, and a four-bladed vane. A laptop computer with ICAR Rheometer software installed was applied to operate the driver, record the torque during the test, and calculate the rheological parameters. The operation and procedure of determining the rheological properties have been explained in other studies [41–43].

The UCS test was performed on an automatic compression testing machine (Model HYE-100) of the capacity 100 kN on 70.7 mm CA-CPB cube specimens. The loading rate was 0.2 kN s^{-1} and the presented results are the average of three specimens.

2.3. Orthogonal Experiment Design

The SC, CAsD, and CD were selected as the factors for the rheological properties and compressive strength of CA-CPB. Specifically, SC is the mass fraction of the solid materials in CA-CPB, CAsD is the mass ratio of CAs to tailings, and the CD represents the mass ratio of cement to the sum of tailings and CAs. The dynamic shear stress (τ_0) and plastic viscosity (μ) were selected to characterize the rheological properties of CA-CPB. The UCSs of the CA-CPB after curing, 3 d, 7 d, 14 d, and 28 d, were used to describe the compressive strength of CA-CPB.

The orthogonal design method is widely applied to analyze multi-factor and multi-level cases using a normalized orthogonal table [44,45]. Here, we employed an orthogonal table represented by the symbol $L_n(r^m)$ in this paper, where L stands for *Latin square*. Here, we recalled that an orthogonal table is a matrix whose number of columns m is that of *factors*, each of which can assume one of r different *levels* (level 1 to level r). The number of rows n and the entries of the table, which correspond to numbers between 1 and r , are chosen in such a way that for any choice of t columns, each t -tuple of levels $\{1, \dots, r\}$ appears in exactly one row in the orthogonal table. The parameter t is usually called the *strength* of the orthogonal table. In our case, we have $m = 3$ factors of $r = 4$ different levels each along with $t = 2$. This gives rise to $n = r^t = 16$ rows or experimental runs. Note that this number compares favorably with the theoretically possible number $4^3 = 64$ of all possible combinations of all levels of all factors. We, here, used the $L_{16}(4^3)$ table as shown in Table 4. The level distributions for SC (%) was 77 (level 1), 78 (level 2), 80 (level 3), and 81 (level 4); for CAsD (%) was 5 (level 1), 10 (level 2), 15 (level 3), and 20 (level 4); and for CD was 1:10 (level 1), 1:8 (level 2), 1:6 (level 3), and 1:4 (level 4).

In each experiment, the test procedure was conducted, as shown in Figure 2. The solid materials were first mixed with tap water to make a CA-CPB slurry according to the values of SC, CAs, CD in Table 4. Then, the rheological properties test of fresh CA-CPB was conducted by the ICAR Rheometer. After the rheology test, the CA-CPB slurry was filled into 70.7 mm × 70.7 mm × 70.7 mm standard tri-molds and the molds were removed after about one day (24 h). Then, the CA-CPB specimens were cured for 2 days, 6 days, 13 days, and 27 days. The curing temperature was 20 °C and the relative humidity was controlled at 90(±2)%. Eventually, the UCS test was performed on a compression testing machine.

Table 4. Orthogonal experimental table $L_{16}(4^3)$.

Experiment Number	Solid Concentration (%)	Coarse Aggregates Dosage (%)	Cement Dosage
1	77 (level 1)	5 (level 1)	1:10 (level 1)
2	77	10 (level 2)	1:8 (level 2)
3	77	15 (level 3)	1:6 (level 3)
4	77	20 (level 4)	1:4 (level 4)
5	78 (level 2)	5	1:8
6	78	10	1:10
7	78	15	1:4
8	78	20	1:6
9	80 (level 3)	5	1:6
10	80	10	1:4
11	80	15	1:10
12	80	20	1:8
13	81 (level 4)	5	1:4
14	81	10	1:6
15	81	15	1:8
16	81	20	1:10

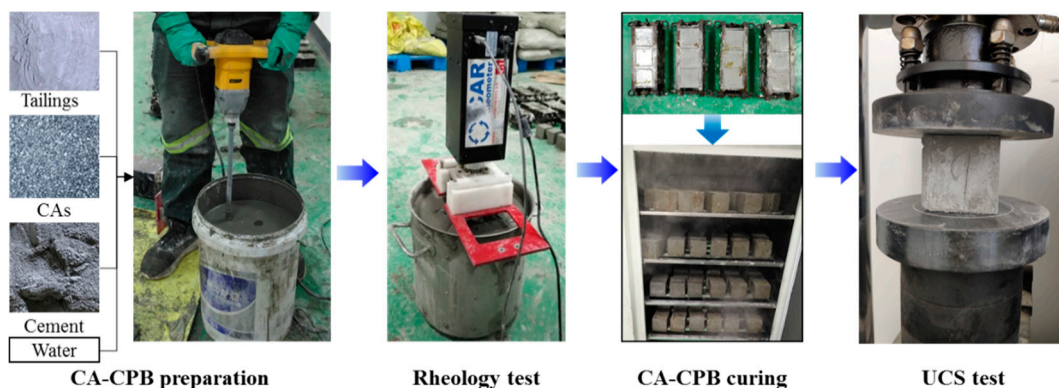


Figure 2. Test procedure.

3. Results and Discussion

3.1. Overall Performance

The experimental results of the rheological properties and UCS tests through the orthogonal experiment design are shown in Table 5 as well as Figures 3 and 4. The value in parentheses after each property in Table 5 is the corresponding coefficient of variation, defined as the ratio of the standard deviation and the average of three specimens [46,47].

Table 5 and Figure 3 illustrate that the rheological properties and UCS of CA-CPB in any experiment are different from those of others. At the same time, τ_0 and μ are in the range of 43.355 to 392.993 Pa and 0.215 to 2.296 Pa s, respectively.

Moreover, Table 5 and Figure 4 show that the UCS of CA-CPB increases over the curing time in each experiment. The evolutions of 3 d UCS, 7 d UCS, 14 d UCS, and 28 d UCS over the curing time are in the same trend.

Table 5. Experimental results of rheological properties and UCS tests.

Experiment Number	τ_0 (Pa)	μ (Pa s)	3 d UCS (MPa)	7 d UCS (MPa)	14 d UCS (MPa)	28 d UCS (MPa)
1	43.36 (18.25)	0.273 (19.97)	0.5 (34.64)	1 (34.64)	1.8 (19.25)	1.9 (9.12)
2	74.32 (19.67)	0.215 (25.14)	0.6 (28.87)	1.3 (13.32)	2.4 (18.16)	2.6 (10.18)
3	89.97 (21.93)	0.254 (18.98)	1.1 (24.05)	2.4 (4.17)	3.5 (7.56)	4.5 (5.88)
4	112.01 (20.95)	0.776 (17.65)	2.6 (7.69)	4.3 (8.39)	6.4 (5.41)	8.1 (2.14)
5	191.54 (21.93)	1.377 (30.03)	0.9 (22.22)	2.1 (12.60)	3.3 (13.21)	3.8 (6.96)
6	136.89 (23.66)	1.004 (26.39)	0.6 (28.87)	1 (20.00)	1.8 (19.25)	1.9 (9.12)
7	112.21 (27.79)	0.843 (22.87)	1.5 (11.55)	3.6 (7.35)	5.5 (6.56)	5.6 (4.72)
8	85.78 (22.30)	0.352 (29.77)	1.2 (22.05)	1.9 (13.93)	3.6 (7.35)	3.8 (9.12)
9	266.66 (20.01)	1.625 (28.18)	1.4 (14.29)	2.8 (9.45)	5.7 (9.28)	5.9 (5.87)
10	299.80 (22.31)	1.705 (28.17)	2.1 (12.60)	4.5 (2.22)	6.5 (5.33)	8.1 (2.14)
11	195.34 (22.95)	1.38 (24.55)	0.6 (16.67)	1.2 (22.05)	2.3 (18.95)	2.4 (14.43)
12	194.52 (25.53)	0.883 (27.06)	0.8 (21.65)	1.7 (11.76)	2.7 (9.80)	3.3 (8.02)
13	392.99 (24.64)	2.296 (22.03)	2.9 (3.45)	5.8 (4.56)	8.5 (6.55)	9.2 (1.09)
14	299.06 (22.07)	1.675 (31.96)	1.7 (5.88)	3.6 (7.35)	5.3 (4.99)	7.4 (3.58)
15	228.89 (21.94)	1.361 (28.26)	1.1 (24.05)	2.1 (12.60)	3.7 (8.11)	4.9 (3.53)
16	197.81 (26.13)	1.024 (22.63)	0.6 (28.87)	1.4 (12.37)	2.4 (11.02)	2.8 (3.57)

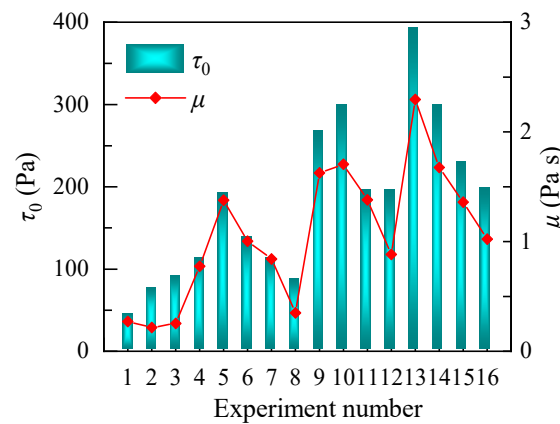


Figure 3. Variation in rheological properties of the orthogonal experiment.

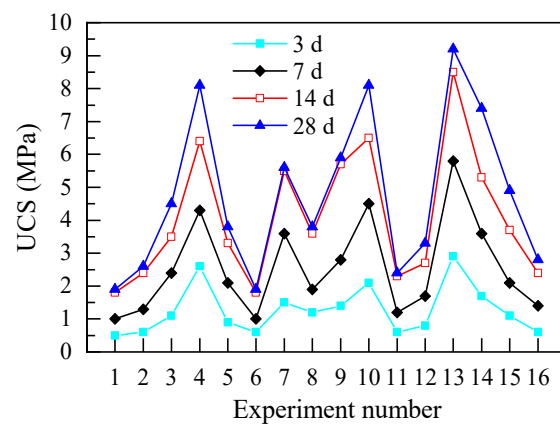


Figure 4. Variation in UCS of the orthogonal experiment.

3.2. Range Analysis of Rheological Properties

Range analysis is widely utilized to evaluate the influence of each factor and obtain the optimal combination [48–52]. In the procedure of range analysis, the range value (R_{y_i-m}) is calculated through Equation (1).

$$R_{y_i-m} = \max(\overline{K_{y_i-m1}}, \overline{K_{y_i-m2}}, \dots, \overline{K_{y_i-mr}}) - \min(\overline{K_{y_i-m1}}, \overline{K_{y_i-m2}}, \dots, \overline{K_{y_i-mr}}), \quad (1)$$

where R_{y_i-m} is the range value of the response y_i under the effect of factor m . The subscript y_1, y_2, \dots, y_6 represent the six responses $\tau_0, \mu, 3 \text{ d CUS}, 7 \text{ d CUS}, 14 \text{ d CUS}$, and 28 d CUS , respectively. The subscript m is the factors A (SC), B (CAdS), and C (CD). At the same time, $\overline{K_{y_i-mr}}$ is the mean of the four responses y_i with the same level r ($r = 1, 2, 3$, and 4) of factor m .

According to the value of R_{y_i-m} , we can determine the importance of each factor on the response y_i . If the R_{y_i-m} value of factor m is bigger than any other factor, factor m has the most significant influence on the response y_i .

Taking y_1 (τ_0) as an example, $\overline{K_{\tau_0-A1}}$ is the mean of the four values of τ_0 with the same level 1 of factor A. It can be found from Table 2 that the four values are 43.355, 74.320, 89.974, and 112.011. Accordingly, $\overline{K_{\tau_0-A1}}$ is 79.91. Similarly, $\overline{K_{\tau_0-A2}}, \overline{K_{\tau_0-A3}}$, and $\overline{K_{\tau_0-A4}}$ are 131.60, 239.08, and 279.68, respectively. Then R_{τ_0-A} can be obtained as 199.77, which is 279.68 minus 79.91. The relation curve of τ_0 with SC is shown in Figure 5a, which illustrates that the mean of τ_0 increases with the increase of SC. This knowledge is well-known in other studies [11,53].

Similarly, the values of R_{τ_0-B} and R_{τ_0-C} are 76.11 and 85.90, respectively. Considering R_{τ_0-A} is the largest among the three range values, A (SC) has the most significant influence on τ_0 . The degree of effect of the factors on τ_0 is $A > C > B$. The relation curves of τ_0 with

A, B, and C are shown in Figure 5. Both the relationships between τ_0 and both A and C are positively linear. On the contrary, the relationship between τ_0 and both A and C is negatively linear. Lower yield stress means higher fluidity, thus the optimal levels of A, B, and C are 1, 4, and 1. Therefore, the optimal combination for τ_0 of CA-CPB is A1C1B4, in which A1, C1, and B4 represent level 1 of A, level of C, and level 4 of B, respectively.

Moreover, Figure 5 demonstrates that the relationships between μ and each factor are similar to those between τ_0 and each factor. The values of $R_{\mu-A}$, $R_{\mu-B}$, and $R_{\mu-C}$ are 1.2095, 0.6340, and 0.4847, indicating that the order of the significant influence of each factor on μ is $A > B > C$. The optimal levels of A, B, and C are 1, 4, and 1, notably the same with τ_0 . The optimal combination for μ is A1B4C1.

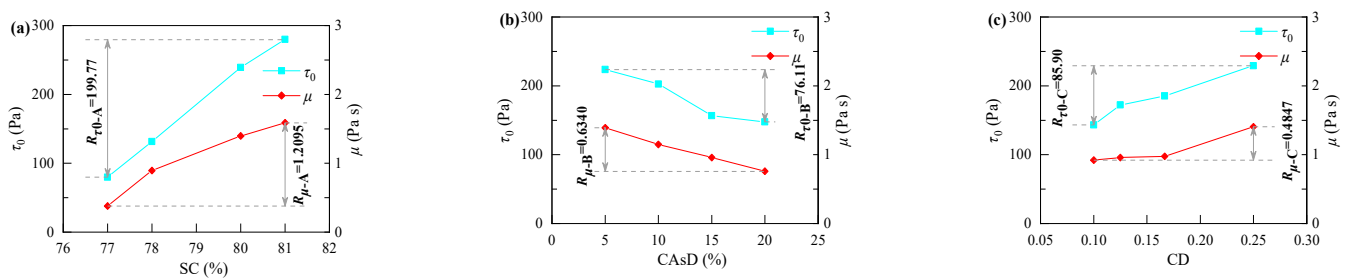


Figure 5. Relation curves of rheological properties with (a) SC (solid concentration), (b) CA sD (coarse aggregates dosage), and (c) CD (cement dosage) by range analysis.

The rheological behaviors of CA-CPB under different SCs and CDs are similar to those of the pure CPB, which were investigated in other studies [11,13]. For CPB, τ_0 and μ decrease with the specific surface area [14]. The specific surface area of CAs is smaller than that of the tailings, thus the increase of CA sD reduces the water holding capacity of CA-CPB. That is to say, a higher dosage of CAs leads to more free water in the CA-CPB, which increases fluidity. Therefore, the dosage of CAs is beneficial for CA-CPB in this study.

3.3. Range Analysis of UCS

According to the range analysis procedure, the relation curves of 3 d UCS, 7 d UCS, 14 d UCS, and 28 d UCS with A (SC), B (CA sD), and C (CD) are shown in Figure 6.

The UCS of CA-CPB obviously varied with all the three factors (SC, CA sD, and CD). Concerning the 3 d UCS, the R_{3d-A} , R_{3d-B} , and R_{3d-C} are 0.675, 0.525, and 1.6, respectively. Therefore, the order of the significant influence of each factor on 3 d UCS is $C > A > B$. In the CPB process, high strength is always desirable. The optimal levels of A, B, and C are 4, 1, and 4, indicating that the optimal combination for 3 d UCS is C4A4B1. Similarly, the optimal combinations for 7 d UCS, 14 d UCS, and 28 d UCS are also C4A4B1.

Moreover, Figure 6a demonstrates that the 3 d UCS first decreased with an increase in SC and then increased for $SC > 78\%$. Additionally, the evolutions of 7 d UCS, 14 d UCS, and 28 d UCS with SC are similar to that of 3 d UCS. Normally, the UCS of CPB is positively correlated with SC [6,10]. The first decrease of UCS in Figure 6a may be because of the effect of CAs. Even though the impact of the CA sD on the UCS is the least significant, UCS first decreased with an increase in CAs and then increased for CAs $> 15\%$, as shown in Figure 6b. Considering that not only the dosage but also the surface morphology and structure of CAs influence the UCS of concrete [54], the relation curves of the UCS of CA-CPB with CA sD are not monotonically increasing or decreasing. Moreover, UCS is mainly ascribed to the formed cementitious products (such as C-S-H gel) by hydration reactions, as the higher the CD, the more cementitious products are formed, resulting in higher UCS [55]. The relationships between 3 d UCS and CD, 7 d UCS and CD, 14 d UCS and CD, and 28 d UCS and CD are almost positively linear in Figure 6c. The variation of the UCS of CA-CPB with CD is similar to that of pure CPB or other concretes [10,39,48,49].

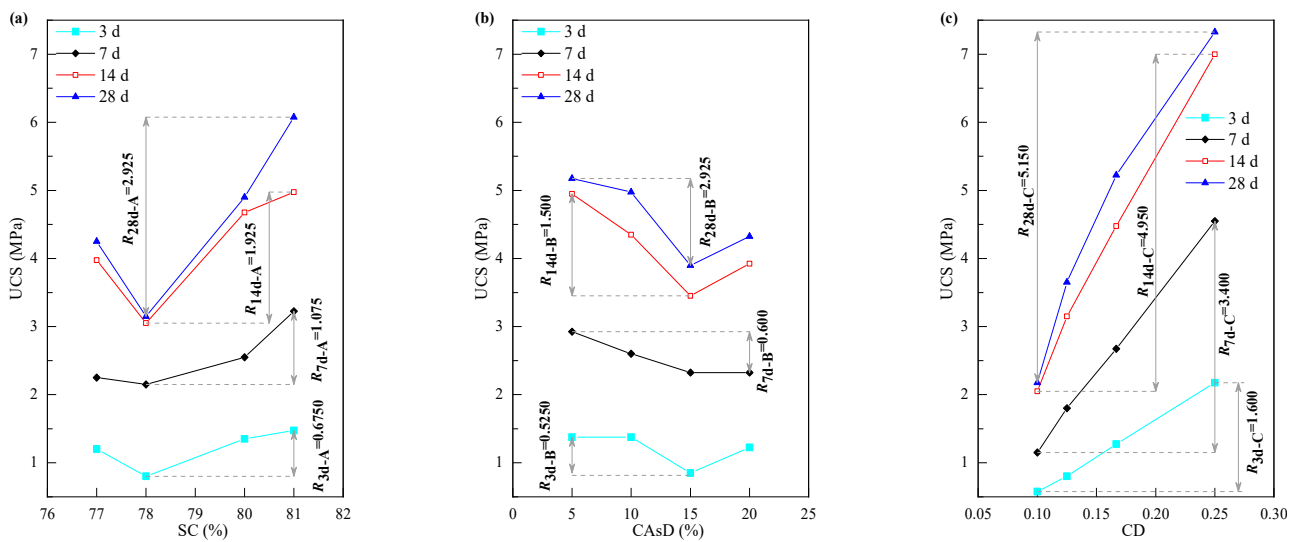


Figure 6. Relation curves of UCS with (a) SC (solid concentration), (b) CAsD (coarse aggregates dosage), and (c) CD (cement dosage) by range analysis.

3.4. Multiple Response Optimization and Validation

Based on the above range analysis, the evolutions of the rheological properties with each factor are different from that of UCS. More seriously, the effect of each factor on the rheological properties is different to that on UCS. The optimal levels of A and C for rheological properties are 1 and 1, whereas that for UCS is 4. At the same time, the optimal level of B for the rheological properties is 4, but that for UCS is 1. The optimal levels of each factor for the rheological properties and UCS are different, resulting in different optimal combinations. It is difficult to achieve the highest UCS and highest fluidity (lowest τ_0 and μ) simultaneously. At the same time, the variations in 3 d UCS, 7 d UCS, 14 d UCS, and 28 d UCS with each factor are similar.

Therefore, τ_0 , μ , and 28 d UCS were selected as the responses for optimizing rheological properties and UCS. The multiple response optimization was conducted through the overall desirability (OD) function approach, which has been employed in other studies [56,57]. Then, the optimal conditions for multiple responses were obtained by maximizing the OD function, as shown in Equation (2).

$$OD = (d_1 \times d_2 \times d_6)^{1/3}, \tag{2}$$

where d_1 , d_2 , and d_6 represent an individual desirability function-converted response y_1 , y_2 , and y_6 , respectively. The scale of d_1 , d_2 , and d_6 ranges from 0 to 1 to the possible values of y_1 , y_2 , and y_6 , where 0 represents that the response is fully unacceptable and 1 illustrates that the response is fully desirable.

The individual desirability functions of d_1 , d_2 , and d_6 are given in Equations (3)–(5).

$$d_1 = \begin{cases} 1 & \text{if } y_1 \leq 43.355, \\ \left(\frac{y_1 - 200}{43.355 - 200}\right)^{0.3} & \text{if } 43.355 < y_1 < 200, \\ 0 & \text{if } y_1 \geq 200. \end{cases} \tag{3}$$

$$d_2 = \begin{cases} 1 & \text{if } y_2 \leq 0.215, \\ \left(\frac{y_2 - 2.296}{0.215 - 2.296}\right)^{0.3} & \text{if } 0.215 < y_2 < 2.296, \\ 0 & \text{if } y_2 \geq 2.296. \end{cases} \tag{4}$$

$$d_6 = \begin{cases} 0 & \text{if } y_6 \leq 1.9, \\ \left(\frac{y_6 - 1.9}{9.2 - 1.9}\right)^{0.3} & \text{if } 1.9 < y_6 < 9.2, \\ 1 & \text{if } y_6 \geq 9.2. \end{cases} \quad (5)$$

where 43.355 in Equation (3) is the minimum value of y_1 in Table 2 and 200 is the upper limit of τ_0 in CPB [58]. The values 0.215 and 2.296 are the minimum and maximum of y_2 in Table 2, respectively. The values 1.9 and 9.2 are the lower and upper limits of y_6 under the given experimental setup, respectively.

The regression models for y_1 , y_2 , and y_6 in the form of a quadratic polynomial equation are shown in Equations (6)–(8).

$$y_1 = -17298.76 + 367.6A + 177.04B + 477.32C - 1.85A^2 + 0.12B^2 + 1493.1C^2 - 2.29AB - 5.15AC - 27.66BC, (R^2 = 0.9509) \quad (6)$$

$$y_2 = -394.73 + 9.3A + 1.76B + 72.56C - 0.05A^2 + 53.61B^2 - 0.02AB - 1.16AC + 0.05BC, (R^2 = 0.9505) \quad (7)$$

$$y_6 = -394.73 + 9.3A + 1.76B + 72.56C - 0.05A^2 + 53.61B^2 - 0.02AB - 1.16AC + 0.05BC, (R^2 = 0.9736) \quad (8)$$

where A , B , and C represent the factor A (SC), B (CA_dS), and C (CD), respectively. The coefficients of determination were 0.9509, 0.9505, and 0.9736, indicating that the regression models are significant.

Finally, the optimal factors estimated were $A = 77\%$, $B = 20\%$, and $C = 0.227$, producing a maximum OD value of 0.9386. Correspondingly, $\tau_0 = 85.129$ Pa, $\mu = 0.469$ Pa s, and 28 d UCS = 6.96 MPa.

Validation experiments were performed under the optimal conditions for an individual response and multiple responses, and the validation results are $\tau_0 = 91.606$ Pa, $\mu = 0.482$ Pa s, and 28 d UCS = 6.5 MPa. The relative errors between predicted and measured values are between -7% and 7% provided that the proposed models are feasible. The optimal parameters above could provide valuable information for the CA-CPB process in the Chifeng Baiyinnuoer Lead and Zinc Mine.

4. Conclusions

This work investigated the influences of solid concentration, coarse aggregates dosage, and cement dosage on the rheological properties and compressive strength of CA-CPB through three-factor and four-level orthogonal tests. The optimization of parameters for the rheological properties and compressive strength of CA-CPB was carried out. As a result, the following conclusions were obtained.

- (1) The effects of solid concentration, coarse aggregates dosage, and cement dosage on rheological properties differ from that on UCS. The most significant influences on rheological properties and UCS are solid concentration and cement dosage, respectively.
- (2) The optimal combinations for rheological properties and UCS are different.
- (3) The overall desirability function is an effective approach for multiple response optimization of CA-CPB.
- (4) The optimal conditions for the high fluidity and high strength of CA-CPB in this study are a solid concentration of 77%, coarse aggregates dosage of 20%, and cement dosage of 0.227, producing τ_0 of 85.129 Pa, μ of 0.469 Pa s, and 28 d UCS of 6.96 MPa.

Author Contributions: Conceptualization, J.W. and Z.R.; methodology, J.W., A.W., Z.R., R.B. and Y.W.; software, Z.R. and S.W.; validation, Z.R. and J.W.; formal analysis, Z.R. and J.W.; investigation, Z.R.; resources, A.W., P.Z. and Z.G.; data curation, J.W.; writing—original draft preparation, J.W. and Z.R.; writing—review and editing, A.W., Z.R., R.B., Y.W. and S.W.; supervision, A.W.; project administration, A.W., P.Z. and Z.G.; funding acquisition, A.W., Z.R. and R.B. All authors have read and agreed to the published version of the manuscript.

Funding: This research study was funded by the National Natural Science Foundation of China (no. 52130404); China Postdoctoral Science Foundation (no. 2021M690011); Guangdong Basic and Applied Basic Research Foundation (no. 2021A1515110161); Postdoctor Research Foundation of Shunde Graduate School of University of Science and Technology Beijing (no.2021BH011); ANID (Chile) through Fondecyt project 1210610; Centro de Modelamiento Matemático (BASAL funds for Centers of Excellence ACE 210010 and FB210005); CRHIAM, project ANID/FONDAP/15130015; and Anillo project ANID/PIA/ACT210030.

Data Availability Statement: Data available on request due to restrictions.

Acknowledgments: The authors acknowledge Zhiyuan Wang, Xiaotian Wang, Yuanfeng Miao, and Yatian Wang for their help in the experiment; and JCHX Mining Management Co., Ltd. for providing experiment equipments.

Conflicts of Interest: The authors declare no conflict of interest.

Abbreviations

CA-CPB	CPB blended with coarse aggregates
CAs	coarse aggregates
CAsD	CAs dosage
CD	cement dosage
CPB	cemented paste backfill
OD	overall desirability
PSD	particle size distribution
SC	solid (tailings, CAs, and cement) concentration
UCS	uniaxial compressive strength
XRF	X-Ray Fluorescence

References

1. Asif, Z.; Chen, Z. Environmental management in North American mining sector. *Environ. Sci. Pollut. Res.* **2016**, *23*, 167–179. [[CrossRef](#)]
2. Wu, D. *Mine Waste Management in China: Recent Development*; Springer: Singapore, 2020; ISBN 978-981-32-9215-4.
3. Qi, C.; Fourie, A. Cemented paste backfill for mineral tailings management: Review and future perspectives. *Miner. Eng.* **2019**, *144*, 106025. [[CrossRef](#)]
4. Lu, H.; Qi, C.; Chen, Q.; Gan, D.; Xue, Z.; Hu, Y. A new procedure for recycling waste tailings as cemented paste backfill to underground stopes and open pits. *J. Clean. Prod.* **2018**, *188*, 601–612. [[CrossRef](#)]
5. Ruan, Z.; Wu, A.; Bürger, R.; Betancourt, F.; Ordoñez, R.; Wang, J.; Wang, S.; Wang, Y. A Population Balance Model for Shear-Induced Polymer-Bridging Flocculation of Total Tailings. *Minerals* **2021**, *12*, 40. [[CrossRef](#)]
6. Yang, L.; Yilmaz, E.; Li, J.; Liu, H.; Jiang, H. Effect of superplasticizer type and dosage on fluidity and strength behavior of cemented tailings backfill with different solid contents. *Constr. Build. Mater.* **2018**, *187*, 290–298. [[CrossRef](#)]
7. Gao, J.; Fourie, A. Spread is better: An investigation of the mini-slump test. *Miner. Eng.* **2015**, *71*, 120–132. [[CrossRef](#)]
8. Li, H.; Wu, A.; Cheng, H. Analysis of conical slump shape reconstructed from stereovision images for yield stress prediction. *Cem. Concr. Res.* **2021**, *150*, 106601. [[CrossRef](#)]
9. Li, W.; Guo, L.; Liu, G.; Pan, A.; Zhang, T. Analytical and experimental investigation of the relationship between spread and yield stress in the mini-cone test for cemented tailings backfill. *Constr. Build. Mater.* **2020**, *260*, 119770. [[CrossRef](#)]
10. Yin, S.; Wu, A.; Hu, K.; Wang, Y.; Zhang, Y. The effect of solid components on the rheological and mechanical properties of cemented paste backfill. *Miner. Eng.* **2012**, *35*, 61–66. [[CrossRef](#)]
11. Zhang, Y.; Gan, D.; Xue, Z.; Lu, H. Novel testing method for thixotropy of paste slurry with respect to influencing factors and rheological parameters. *Adv. Powder Technol.* **2021**, *32*, 4744–4753. [[CrossRef](#)]
12. Wu, D.; Yang, B.; Liu, Y. Pressure drop in loop pipe flow of fresh cemented coal gangue-fly ash slurry: Experiment and simulation. *Adv. Powder Technol.* **2015**, *26*, 920–927. [[CrossRef](#)]
13. Panchal, S.; Deb, D.; Sreenivas, T. Variability in rheology of cemented paste backfill with hydration age, binder and superplasticizer dosages. *Adv. Powder Technol.* **2018**, *29*, 2211–2220. [[CrossRef](#)]
14. Adiguzel, D.; Bascetin, A. The investigation of effect of particle size distribution on flow behavior of paste tailings. *J. Environ. Manag.* **2019**, *243*, 393–401. [[CrossRef](#)] [[PubMed](#)]
15. Cheng, H.; Wu, S.; Li, H.; Zhang, X. Influence of time and temperature on rheology and flow performance of cemented paste backfill. *Constr. Build. Mater.* **2020**, *231*, 117117. [[CrossRef](#)]
16. Xu, W.; Zhang, Y.; Zuo, X.; Hong, M. Time-dependent rheological and mechanical properties of silica fume modified cemented tailings backfill in low temperature environment. *Cem. Concr. Compos.* **2020**, *114*, 103804. [[CrossRef](#)]

17. Wu, D.; Fall, M.; Cai, S.J. Coupling temperature, cement hydration and rheological behaviour of fresh cemented paste backfill. *Miner. Eng.* **2013**, *42*, 76–87. [[CrossRef](#)]
18. Ouattara, D.; Yahia, A.; Mbonimpa, M.; Belem, T. Effects of superplasticizer on rheological properties of cemented paste backfills. *Int. J. Miner. Process.* **2017**, *161*, 28–40. [[CrossRef](#)]
19. Xu, W.; Chen, W.; Tian, M.; Guo, L. Effect of temperature on time-dependent rheological and compressive strength of fresh cemented paste backfill containing flocculants. *Constr. Build. Mater.* **2021**, *267*, 2020–2021. [[CrossRef](#)]
20. Zhao, Y.; Taheri, A.; Karakus, M.; Chen, Z.; Deng, A. Effects of water content, water type and temperature on the rheological behaviour of slag-cement and fly ash-cement paste backfill. *Int. J. Min. Sci. Technol.* **2020**, *30*, 271–278. [[CrossRef](#)]
21. Yang, L.; Wang, H.; Wu, A.; Li, H.; Tchamba, A.B.; Bier, T.A. Shear thinning and thickening of cemented paste backfill. *Appl. Rheol.* **2019**, *29*, 80–93. [[CrossRef](#)]
22. Ruan, Z.; Wu, A.; Bürger, R.; Betancourt, F.; Wang, Y.; Wang, Y.; Jiao, H.; Wang, S. Effect of interparticle interactions on the yield stress of thickened flocculated copper mineral tailings slurry. *Powder Technol.* **2021**, *392*, 278–285. [[CrossRef](#)]
23. Deng, X.; Zhang, J.; Klein, B.; Zhou, N.; deWit, B. Experimental characterization of the influence of solid components on the rheological and mechanical properties of cemented paste backfill. *Int. J. Miner. Process.* **2017**, *168*, 116–125. [[CrossRef](#)]
24. Tariq, A.; Yanful, E.K. A review of binders used in cemented paste tailings for underground and surface disposal practices. *J. Environ. Manag.* **2013**, *131*, 138–149. [[CrossRef](#)]
25. Cheng, H.; Wu, S.; Zhang, X.; Li, J. A Novel Prediction Model of Strength of Paste Backfill Prepared from Waste-Unclassified Tailings. *Adv. Mater. Sci. Eng.* **2019**, *2019*, 3574190. [[CrossRef](#)]
26. Wu, A.; Wang, Y.; Wang, H.; Yin, S.; Miao, X. Coupled effects of cement type and water quality on the properties of cemented paste backfill. *Int. J. Miner. Process.* **2015**, *143*, 65–71. [[CrossRef](#)]
27. Cao, G.; Wei, Z.; Wang, W.; Zheng, B. Shearing resistance of tailing sand waste pollutants mixed with different contents of fly ash. *Environ. Sci. Pollut. Res.* **2020**, *27*, 8046–8057. [[CrossRef](#)]
28. Qiu, J.; Guo, Z.; Yang, L.; Jiang, H.; Zhao, Y. Effect of tailings fineness on flow, strength, ultrasonic and microstructure characteristics of cemented paste backfill. *Constr. Build. Mater.* **2020**, *263*, 120645. [[CrossRef](#)]
29. Dong, Q.; Liang, B.; Jia, L.; Jiang, L. Effect of sulfide on the long-term strength of lead-zinc tailings cemented paste backfill. *Constr. Build. Mater.* **2019**, *200*, 436–446. [[CrossRef](#)]
30. Sun, W.; Wu, A.; Wang, H.; Li, T.; Liu, S. Experimental study on the influences of sodium sulphide on zinc tailings cement paste backfill in Huize Lead-Zinc Mine. *Int. J. Min. Miner. Eng.* **2015**, *6*, 119–138. [[CrossRef](#)]
31. Chen, S.; Wu, A.; Wang, Y.; Wang, W. Coupled effects of curing stress and curing temperature on mechanical and physical properties of cemented paste backfill. *Constr. Build. Mater.* **2021**, *273*, 121746. [[CrossRef](#)]
32. Yao, G.; Cui, T.; Zhang, J.; Wang, J.; Lyu, X. Effects of mechanical grinding on pozzolanic activity and hydration properties of quartz. *Adv. Powder Technol.* **2020**, *31*, 4500–4509. [[CrossRef](#)]
33. Fu, J.; Wang, J.; Song, W. Damage constitutive model and strength criterion of cemented paste backfill based on layered effect considerations. *J. Mater. Res. Technol.* **2020**, *9*, 6073–6084. [[CrossRef](#)]
34. Koohestani, B.; Bussi ere, B.; Belem, T.; Koubaa, A. Influence of polymer powder on properties of cemented paste backfill. *Int. J. Miner. Process.* **2017**, *167*, 1–8. [[CrossRef](#)]
35. Yu, B.; Chen, Y.; Liu, Q. Experimental study on the influence of coarse particle on the yield stress of debris flows. *Appl. Rheol.* **2016**, *26*, 10–12. [[CrossRef](#)]
36. Mahaut, F.; Mok eddem, S.; Chateau, X.; Roussel, N.; Ovarlez, G. Effect of coarse particle volume fraction on the yield stress and thixotropy of cementitious materials. *Cem. Concr. Res.* **2008**, *38*, 1276–1285. [[CrossRef](#)]
37. Choi, M.S. Numerical prediction on the effects of the coarse aggregate size to the pipe flow of pumped concrete. *J. Adv. Concr. Technol.* **2014**, *12*, 239–249. [[CrossRef](#)]
38. Vishalakshi, K.P.; Revathi, V.; Sivamurthy Reddy, S. Effect of type of coarse aggregate on the strength properties and fracture energy of normal and high strength concrete. *Eng. Fract. Mech.* **2018**, *194*, 52–60. [[CrossRef](#)]
39. Sun, W.; Wang, H.; Hou, K. Control of waste rock-tailings paste backfill for active mining subsidence areas. *J. Clean. Prod.* **2018**, *171*, 567–579. [[CrossRef](#)]
40. Wu, J.; Yin, Q.; Gao, Y.; Meng, B.; Jing, H. Particle size distribution of aggregates effects on mesoscopic structural evolution of cemented waste rock backfill. *Environ. Sci. Pollut. Res.* **2021**, *28*, 16589–16601. [[CrossRef](#)]
41. Durgun, M.Y.; Atahan, H.N. Rheological and fresh properties of reduced fine content self-compacting concretes produced with different particle sizes of nano SiO₂. *Constr. Build. Mater.* **2017**, *142*, 431–443. [[CrossRef](#)]
42. Li, H.; Huang, F.; Xie, Y.; Yi, Z.; Wang, Z. Effect of water–powder ratio on shear thickening response of SCC. *Constr. Build. Mater.* **2017**, *131*, 585–591. [[CrossRef](#)]
43. Sethy, K.P.; Pasla, D.; Chandra Sahoo, U. Utilization of high volume of industrial slag in self compacting concrete. *J. Clean. Prod.* **2016**, *112*, 581–587. [[CrossRef](#)]
44. Gui, L.; Long, M.; Chen, D.; Zhao, J.; Wang, Q.; Duan, H. Thermodynamic study on the solute partition coefficients on L/δ and L/δ+γ phase interfaces for 1215 high-sulfur steel solidification by orthogonal design. *J. Mater. Res. Technol.* **2020**, *9*, 89–103. [[CrossRef](#)]
45. Fu, Q.; Xu, W.; Bu, M.X.; Guo, B.; Niu, D. Orthogonal experimental study on hybrid-fiber high-durability concrete for marine environment. *J. Mater. Res. Technol.* **2021**, *13*, 1790–1804. [[CrossRef](#)]

46. Adeosun, J.T.; Lawal, A. Numerical and experimental studies of mixing characteristics in a T-junction microchannel using residence-time distribution. *Chem. Eng. Sci.* **2009**, *64*, 2422–2432. [[CrossRef](#)]
47. Guo, G.; Fall, M. Modelling of preferential gas flow in heterogeneous and saturated bentonite based on phase field method. *Comput. Geotech.* **2019**, *116*, 103206. [[CrossRef](#)]
48. Zheng, G.; Huang, J.; Diao, Y.; Ma, A.; Su, Y.; Chen, H. Formulation and performance of slow-setting cement-based grouting paste (SCGP) for capsule grouting technology using orthogonal test. *Constr. Build. Mater.* **2021**, *302*, 124204. [[CrossRef](#)]
49. Zhao, Y.; Liang, N.X.; Chen, H.; LI, Y. Preparation and properties of sintering red mud unburned road brick using orthogonal experiments. *Constr. Build. Mater.* **2020**, *238*, 117739. [[CrossRef](#)]
50. Yao, C.; Guo, Y.; Shen, A.; Cui, W.; He, Z. Recycling of fine-asphalt-pavement solid waste for low-shrinkage rapid hardening Portland cement concrete pavement. *Constr. Build. Mater.* **2021**, *289*, 123132. [[CrossRef](#)]
51. Xia, Q.; Wen, J.; Tang, X.; Zhu, Y.; Xu, Z.; Du, Z.; Liu, X. Optimal preparation and degradation characterization of repair mortar containing waterborne epoxy resin emulsions. *Constr. Build. Mater.* **2021**, *298*, 123839. [[CrossRef](#)]
52. Fang, Y.; Ma, B.; Wei, K.; Wang, L.; Kang, X.X.; Chang, X.G. Orthogonal experimental analysis of the material ratio and preparation technology of single-component epoxy resin for asphalt pavement crack repair. *Constr. Build. Mater.* **2021**, *288*, 123074. [[CrossRef](#)]
53. Wu, A.; Wang, Y.; Wang, H. Estimation model for yield stress of fresh uncemented thickened tailings: Coupled effects of true solid density, bulk density, and solid concentration. *Int. J. Miner. Process.* **2015**, *143*, 117–124. [[CrossRef](#)]
54. Jia, J.; Gu, X. Effects of coarse aggregate surface morphology on aggregate-mortar interface strength and mechanical properties of concrete. *Constr. Build. Mater.* **2021**, *294*, 123515. [[CrossRef](#)]
55. He, Y.; Zhang, Q.; Chen, Q.; Bian, J.; Qi, C.; Kang, Q.; Feng, Y. Mechanical and environmental characteristics of cemented paste backfill containing lithium slag-blended binder. *Constr. Build. Mater.* **2021**, *271*, 121567. [[CrossRef](#)]
56. Mondal, B.; Srivastava, V.C.; Mall, I.D. Electrochemical treatment of dye-bath effluent by stainless steel electrodes: Multiple response optimization and residue analysis. *J. Environ. Sci. Health Part A* **2012**, *47*, 2040–2051. [[CrossRef](#)] [[PubMed](#)]
57. Wu, A.; Ruan, Z.; Bürger, R.; Yin, S.; Wang, J.; Wang, Y. Optimization of flocculation and settling parameters of tailings slurry by response surface methodology. *Miner. Eng.* **2020**, *156*, 106488. [[CrossRef](#)]
58. Ouattara, D.; Mbonimpa, M.; Yahia, A.; Belem, T. Assessment of rheological parameters of high density cemented paste backfill mixtures incorporating superplasticizers. *Constr. Build. Mater.* **2018**, *190*, 294–307. [[CrossRef](#)]